PLA aerogel as a universal support for the typical organic phase change energy storage materials

Guang-Zhong Yin, [a, b, *] Xiao-Mei Yang, [b] Alba Marta López, [b] Xiang Ao, [b] Mei-Ting Wang, [c] Javier García Molleja, [b] De-Yi Wang [a, b, *]

[a] *Escuela Politécnica Superior, Universidad Francisco de Vitoria, Ctra. Pozuelo-Majadahonda Km 1.800, 28223, Pozuelo de Alarcón, Madrid, Spain*

[b] *IMDEA Materials Institute, C-Eric Kandel, 2, 28906 Getafe, Madrid, Spain*

[c] *Liaoning Provincial key Laboratory for Preparation and Application of Special Functional Materials, Shenyang University of Chemical Technology, Shenyang 110142, China*

Corresponding Authors

*Tel: +34 615664438; Email: amos.guangzhong@ufv.es
*Tel: +34 91 549 34 22, fax: +34 91 550 30 47; Email: deyi.wang@imdea.org

Abstract

We first prepared Polylactic acid (PLA) aerogels with high porosity based on a facile and efficient thermal induced phase separation technique. In view of the excellent internal nano structure of PLA aerogel, high porosity and suitable interfacial affinity, it was selected as a support material to encapsulate four common organic phase change materials (PCMs), thereby preparing anti-leakage, shape-stable and sustainable PCMs with ultra-high latent heat (178.9-224.9 J g^{-1}). PLA aerogel encapsulated PCMs perform high enthalpy efficiency (>92 %), which may benefit from the highly internal compatible nanostructure of PLA. Thermally conductive fillers (Boron nitride and Graphene nanoplatelet) were introduced to improve thermal conductivity. An important factor of PLA aerogel as a universal encapsulation matrix is analyzed based on the solubility parameters and Flory-Huggins parameters. The application cases of smart container and thermal regulation in

confined spaces further prove the practical application value in the thermal regulation and energy saving area.

Keywords: Phase change materials; PLA; Aerogel; Energy storage materials; Nanocomposites

1. Introduction

The increasingly prominent energy and environmental problems are pushing the requirements of our society for improved energy conservation and environmental protection. The requirements for efficient energy use are also increasingly higher. Thermal energy storage (TES) technologies are valuable components in many energy systems and could be an important tool in achieving a low-carbon future. [1,2] According to the storage principle, TES technologies can be divided into three categories: sensible heat storage, latent heat storage and thermochemical heat storage. Latent heat storage technologies based on Phase change materials (PCMs) are particularly attractive for applications where thermal energy must be stored or delivered over a narrow temperature range or when compactness is a requirement. [3,4]

During the development of PCMs, many kinds of materials have been deeply studied, including inorganic compounds (salts and hydrated salts) and organic compounds, such as, paraffins,[5,6] fatty acids,[7] and polyethylene glycols (PEGs).[8] Generally, the ideal PCMs should satisfy the required thermophysical and chemical properties, such as suitable phase transition temperature, high energy storage density, good thermal conductivity, anti-leakage, shape-stability and both good chemical and cycling stability.

Most widely used organic PCMs undergo solid-liquid transitions. However, solid-liquid PCMs require encapsulation in order to avoid leakage of the liquid phase at temperatures above the melting point which may limit the practical use of PCMs. At present, there are various methods that try to solve the leakage problem of PCMs, which generally consist of porous solid supports capable of PCMs entrapment. [9] Methods for obtaining leakage-free materials include the adsorption method,[10] microencapsulation method,[11] sol-gel method,[12] or the chemical method.[13]

Common porous materials for adsorption method include clay minerals, porous carbon materials,[14] and metal foams,[15] polysaccharide-based aerogels [16] and other polymeric matrix. [17,18]

As well known, Polylactic acid (PLA) is with the typical major advantages of: (1) 100% biodegradable, compostable, eco-friendly material; (2) good mechanical and physical properties; (3) good compatibility and degradability; and (4) safe and non-toxic. It is mentioned that PLA is a sustainable biodegradable polyester with environmentally friendly characteristics and potential applications for biomedical uses. As our best of knowledge, PLA-encapsulated PCM is rarely reported. In view that the confinement of PCM within 3D porous structure such as aerogel has been identified as the most attractive and efficient strategy to fabricate high performance shape stable PCMs, especially for ensuring the high latent heat.

In the present work, we therefore will select sustainable PLA aerogel as the support material, aiming to fabricate biobased high performance PCMs. There are several well reported technics to prepare PLA-based aerogel (or PLA based highly porous materials). Among the methods, the phase separation technique conventionally divides into thermal induced phase separation (TIPS) [19] and nonsolvent induced phase separation (NIPS) [20,21]. In current work, we will use a revised TIPS method for the aerogel fabrication. Subsequently, we will analyze the preparation, morphology and porosity of the aerogels, realize the effective encapsulation of four conventional PCM work substances (Paraffin (hydrocarbons), PEG (ethers), Stearic acid (acids) and Stearyl alcohols (alcohols)), and finally analyze the optimality of PLA aerogel based on the Flory-Huggins parameter.

2. Results and discussion

2.1 Preparation of PLA aerogels

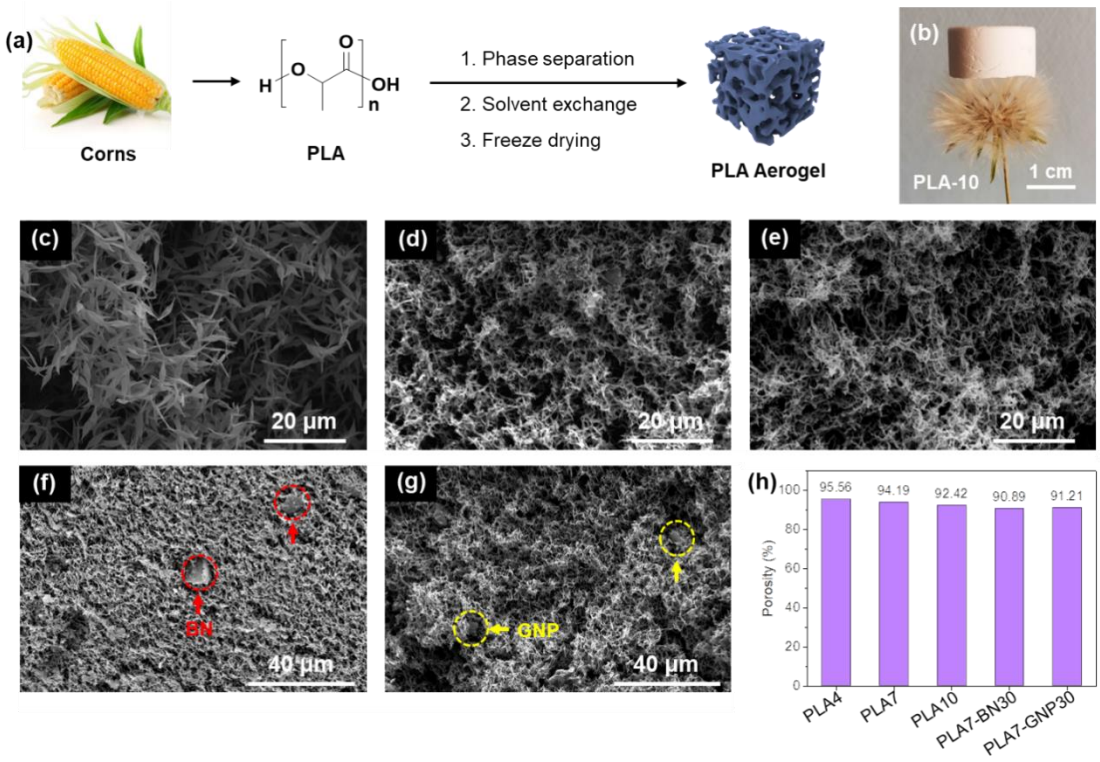

Figure 1. (a) Illustration of biomass-derived PLA aerogel fabrication, (b) PLA 10 was selected as a typical example to show the lightweight nature of the aerogel, (c) Scanning Electron Microscope (SEM) image of sample PLA 4, (d) SEM image of sample PLA 7, (e) SEM image of sample PLA 10, (f) SEM image of sample PLA 7 with Boron Nitride as fillers, (g) SEM image of sample PLA 7 with Graphene Nanoplatelet as fillers and (h) porosities of the aerogels. The porosity values are calculated according to Eq. (1).

As shown in **Figure 1a**, we selected biomass-derived PLA to prepare aerogels by a three-step strategy, namely, (1) thermal induced phase separation, (2) solvent exchange and (3) freeze drying. The specific experimental procedures were systematically provided in Supplementary data (see the experimental section). As reported, 0.03 g mL^{-1} was the minimum critical concentration. [21] We therefore chose 0.04 g mL^{-1}, 0.07 g mL^{-1} and 0.10 g mL^{-1} of PLA in acetone, and accomplished phase separation at -20 °C, the acetone was then fully replaced with water. Followed by

lyophilization, PLA aerogels (e.g., PLA4, PLA7, and PLA10) with different micro-nano morphology and porosities were obtained. We selected sample PLA 10 as a typical example to demonstrate its appearance and lightweight nature (**Figure 1b**). Notably, it is conveniently to fabricate the PLA aerogel in large scale. As shown in **Figure S1a**, we obtained the PLA aerogel with size of 33 cm×19 cm, which provides the possibility for large-scale production in the future, so as to the practical application in construction materials. Furthermore, the aerogel can be conveniently cut for determined size and shapes (**Figure S1b**).

The images of the remaining aerogel samples (PLA4, PLA7, PLA7-BN30 and PLA7-GNP30) are all shown in **Figure S1c**. The concentration of PLA can affect the rate of phase separation, thereby affecting the microscopic morphology as well as the porosity. As shown in **Figure 1c-e**, the sample presented a petal-like nano sheet (**Figure 1c** for PLA4 with low concentration). As the concentration increased, the fibrous nano structures were formed (**Figure 1d, 1e**). Specifically, for example, sample PLA10 basically exhibits a nanofiber-like microscopic morphology. Boron Nitride (BN) and Graphene nanoplatelets (GNP) can be introduced into the aerogel framework for improving the thermal conductivity. As shown in **Figure 1f** and **g**, the fillers were well dispersed in the aerogels. We calculated the porosity of the aerogel based on **Eq. 1**:[22]

$$Porosity\% = \frac{\rho_{bulk} - \rho_{porous}}{\rho_{bulk}} \times 100\% \quad (1)$$

where, ρ_{porous} is the density of porous materials, ρ_{bulk} is the density of bulk PLA with value of 1.24 g mL^{-1} according to the product data sheet. The corresponding densities results are all summarized in **Table 1**.

It can be seen that the porosity of PLA4 is the highest with value of 95.56%. The porosity gradually decreased with increasing of PLA concentration. Typically, the porosity of PLA7 and

PLA10 are 94.19% and 92.42%, respectively. When thermal conductive fillers are introduced, the porosity will further decrease, specifically, the porosity of PLA7-BN30 and PLA7-GNP30 decreases to 90.89 % and 91.21 %, respectively.

2.2 Encapsulation of typical PCMs by PLA aerogels

The PLA-based aerogels were further used as the encapsulation matrix of typical PCM work substances (Paraffin (hydrocarbons), PEG (ethers), Stearic acid (acids) and Stearyl alcohols (alcohols), etc.) to prepare a series of shape-stable PCMs (**Figure 2a**). Based on **Eq. 2**, we can calculate the encapsulation ratio as shown in **Figure 2b**.

$$PCM\ loading\ \% = \frac{m_{PCM} - m_{aerogel}}{m_{PCM}} \times 100\% = \frac{\rho_{PCM} - \rho_{foam}}{\rho_{PCM}} \times 100\% \quad (2)$$

where, m_{PCM} and $m_{aerogel}$ are the weight of the final PCM composites and the corresponding aerogel, respectively; ρ_{PCM} is the density of the final PCM composites, and $\rho_{aerogel}$ is the density of the aerogel. The specific calculation indicators are listed in **Table 1**. We further find the PCM loading increases almost linearly with the increase of porosity (**Figure 2c**) by following the linear function:

$$\text{PCM loading (\%)} = 1.47\ \text{Porosity (\%)} - 45.83,\ R^2 = 0.993 \quad (3)$$

Specifically, PLA4 with the highest porosity and has the highest encapsulation ratio of 94.78% accordingly. In addition, the two samples with fillers (namely, sample PLA7-Paraffin-BN30 and PLA7-Paraffin-GNP30) had the lowest encapsulation ratios with values of 88.12 % and 89.12 %, respectively. We then used SEM to observe the internal structure of the PCM composites, as shown in **Figures 2d** to **2k**. There were no significant differences in the cross-sectional morphologies and no phase separation, no caracks observation for all the samples. This may be due to the nanostructure of PLA and the intrinsic properties (e.g., solubility parameter) of PLA, which ensure a good

compatibility between PLA aerogels with the four PCM work substances, resulting in good interfacial wettability. Therefore, no interfacial separation between PLA nano units and PCM work substance was observed. This will be further analyzed in *section 2.4*. In particular, the microstructure of PLA can be clearly seen in the SEM, and the surface protrusions in **Figure 2j** are particularly prominent. Except for sample PLA7-PEG (because PEG is water soluble), the remaining three type of PCM samples have good hydrophobicity, which can maintain the moisture resistance properties of the material to a certain extent, as shown in **Figure 2l**. This is mainly because PLA itself and the three PCMs (Paraffin, stearic acid and stearyl alcohol) are hydrophobic compounds. The hydrophobicity of the material can well meet the waterproof requirements of the material and has a significant advantage in expanding the application environment of the material. The potential advantage of the PLA-PEG based PCM sample is that the separation of aerogel and PEG can be easily achieved. This provides technical possibilities for sample recovery and recycling, because we can easily achieve the effective separation of PEG and PLA by water immersion during the recycling process.

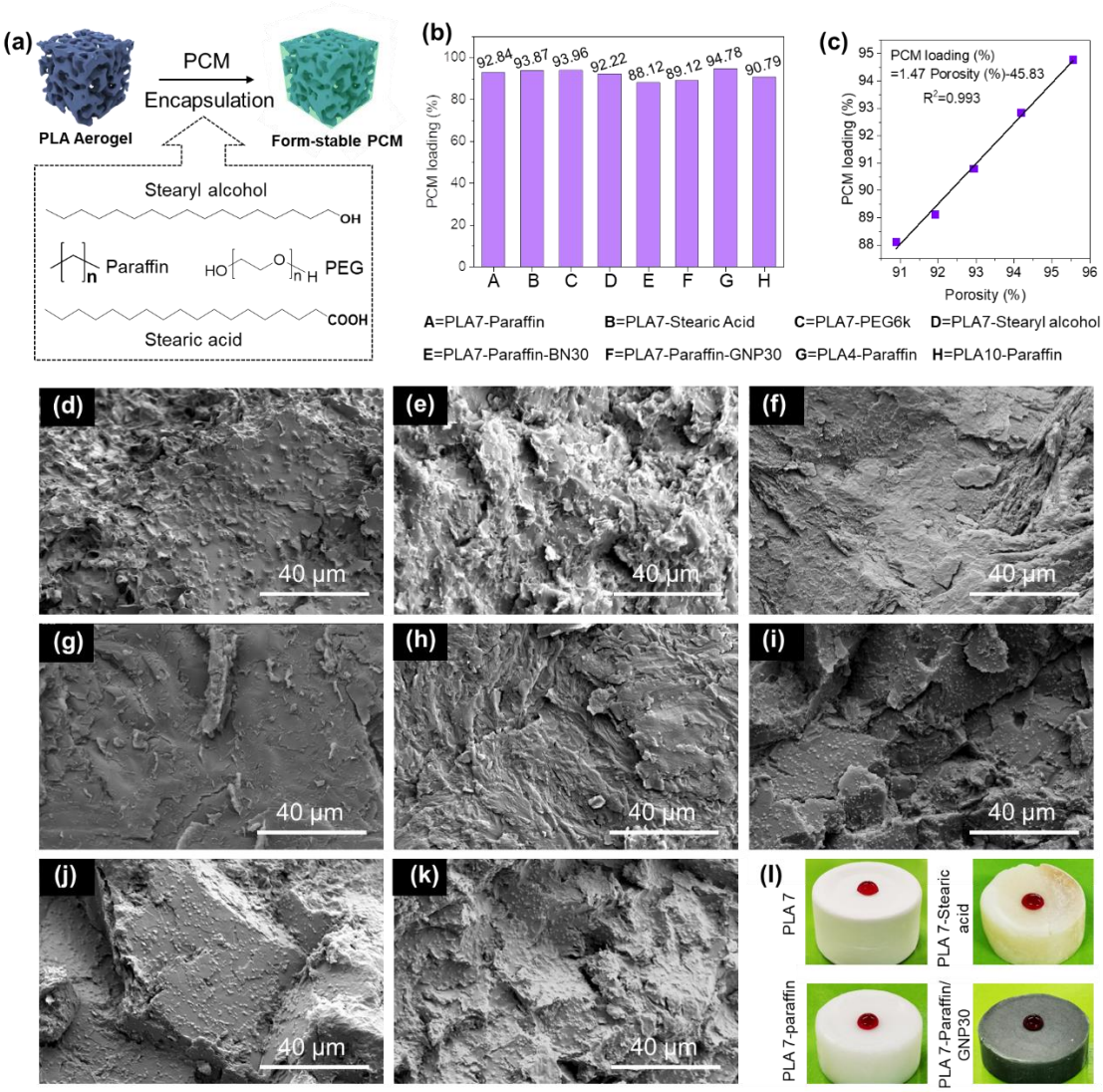

Figure 2. (a) The chemical structure of the four PCM work substances involved in current report, and illustration on the PCM encapsulation, (b) PCM loading % results, (c) linear correlation between PCM loading (%) and porosity (%), (d) cross section SEM image of PLA7-paraffin, (e) cross section SEM image of PLA7-stearic acid, (f) cross section SEM image of PLA7-PEG, (g) cross section SEM image of PLA7-stearyl alcohol, (h) cross section SEM image of PLA7-paraffin-BN30, (i) cross section SEM image of PLA7-paraffin-GNP 30, (j) cross section SEM image of PLA4-paraffin, (k) cross section SEM image of PLA10-paraffin, and (l) Schematic diagram of a hydrophobic surface for the typical samples: Aqueous solution of phenolphthalein drops on the upper surface of sample PLA7, PLA7-Stearic acid, PLA7-Paraffin and PLA7-Paraffin-GNP30.

Table 1. Typical parameters of the PCMs

Samples	Density ($g\ mL^{-1}$)	PCM loading rate (%)	ΔH_m ($J\ g^{-1}$) [a]	ΔH_s ($J\ g^{-1}$) [a]	$T_{m,\ peak}$ (C^o) [a]	$T_{s,\ peak}$ (C^o) [a]	Enthalpy efficiency (%)
Paraffin	-	-	212.1	210.6	67.97	63.90	-
PEG 6K	-	-	222.6	217.4	62.03	38.26	-
Stearyl alcohol	-	-	265.1	262.5	59.23	54.48	-
Stearic Acid	-	-	235.3	234.7	71.35	64.76	-
PLA 7-Paraffin	1.006±0.007	92.84	199.3	199.1	70.31	60.62	[b] 101.21
PLA 7-Stearic acid	1.175±0.008	93.87	203.9	202.8	75.98	64.31	92.31
PLA 7-PEG 6K	1.192±0.048	93.96	209.3	211.7	68.17	59.59	[b] 100.07
PLA 7- Stearyl alcohol	0.925±0.009	92.22	224.9	219.4	65.46	48.58	92.00
PLA 7-Paraffin-BN30	0.951±0.024	88.12	178.9	176,4	70,16	58.76	95.72
PLA 7-Paraffin-GNP30	1.002±0.013	89.12	185.8	183.8	69.42	60.24	98.29
PLA 4-Paraffin	0.884±0.022	94.78	209.0	207.1	69.78	60.31	[b] 103.97
PLA 10-Paraffin	1.021±0.016	90.79	188.5	185.8	70.35	58.76	97.88

Note: a. All the original DSC curves are provided in Supplementary data (**Figure S2-12**); b. The values are higher than 100 % but almost 100 %. This is within an acceptable margin of experimental error.

2.3 Phase change performance of the form-stable PCMs

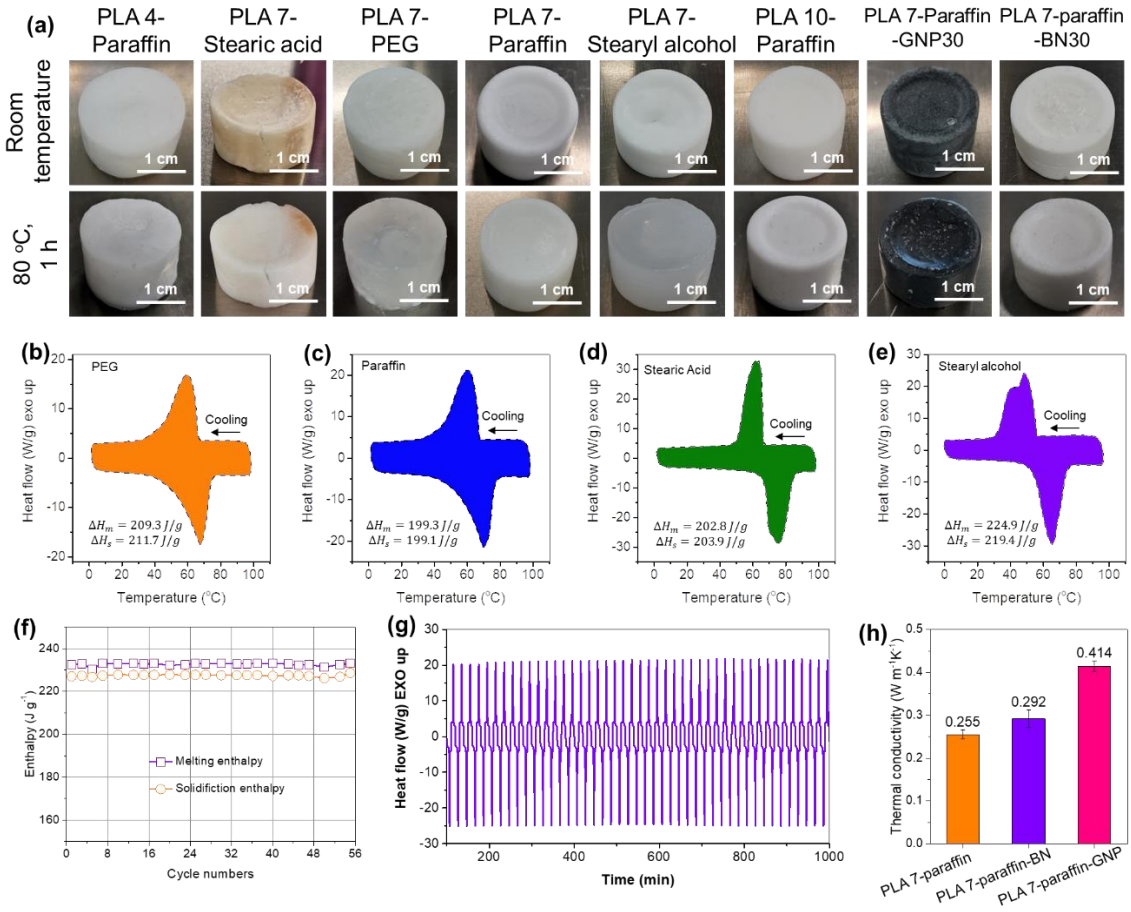

Figure 3. (a) Schematic diagram of form stability test for representative samples: PLA4-Paraffin, PLA7-Stearic acid, PLA7-PEG, PLA7-Paraffin, PLA7-Stearyl alcohol, PLA10-Paraffin, PLA7-Paraffin-GNP30, and PLA7- Paraffin-BN30, (b) DSC cycle of PLA7-PEG, (c) DSC cycle of PLA7-Paraffin, (d) DSC cycle of PLA7-Stearic acid, (e) DSC cycle of PLA7-Stearyl alcohol, (f) Melting enthalpies and solidification enthalpies during the cycle performance test, and (g) DSC curve of PLA 7-paraffin after 55 times heating-cooling cycling (heat flow *vs.* time), (h) thermal conductivity results of sample PLA 7-paraffin, PLA 7-paraffin-BN30, and PLA 7-paraffin-GPN30.

X-ray diffraction (XRD) was recorded to reveal the crystallization patterns of the composite PCMs as shown in **Figure S13**. Encapsulation in PLA had no significant effect on the crystallization of the phase change work substances. All PLA-encapsulated samples showed almost the same XRD curves

as the pristine PCM work substances. The only significant difference is the (110)/(200) planes of the PLA aerogel appear in the all PLA-encapsulated samples. Fourier transform infrared spectrometer (FTIR) curves are all provided in **Figure S14**. Because PLA aerogel and PCM work substances have no chemical reaction or chemical interaction, most of PLA encapsulated samples have almost the same FTIR spectra as that of original PCM work substances. The only significant difference is the signal of the carbonyl group in PLA at 1755 cm^{-1} appeared for all the PLA encapsulated samples. Based on Thermogravimetric analysis (TGA) results (**Figure S15**), we found that all PCMs are stable below 150 ^{o}C. Organic phase change materials are usually used below 100 ^{o}C. Therefore, we can consider that the material is sufficiently stable during the real service of PCM.

We treated the encapsulated samples in an oven at 80 ^{o}C for 1 h, and observed that the samples almost kept the original shape, as shown in **Figure 3a**, and all have good leakage resistance. For a typical example, it can be seen that the retention ratio of sample PLA 10-Paraffin is still 96.7% quality retention after continuous heating for 1 hour (supported by filter paper), as shown in the **Figure S16**. In addition, except for sample PLA4-paraffin, all the samples performed outstanding shape stabilities. Sample PLA4 aerogel shrinks in size (in both encapsulation step and form stability test) to a certain extent after thermal adsorption of PCM due to its poor microscopic continuity (Figure 1c), which indicates that the concentration of PLA should be controlled above 0.04 g mL^{-1} for preparing perfect shape-stable PCMs. It is also the main reason why we choose PLA 7 (with concentration of 0.07 g mL^{-1}) for the follow-up research sample fabrication.

Figure 3b to **3e** present the DSC curves for samples PLA 7-Paraffin, PLA 7-Stearic acid, PLA 7-PEG and PLA 7-Stearyl alcohol. As it can be seen, sample PLA 7-Paraffin, PLA 7-Stearic acid, PLA 7-PEG and PLA 7-Stearyl alcohol have ultra-high latent heat values of 199.3 J g^{-1}, 202.8 J g^{-1}, 209.3

J g^{-1} and 224.9 J g^{-1}, respectively. The specific indicators of all the samples, such as melting enthalpies, solidification enthalpies, melting temperature, enthalpy efficiency, etc., are also shown in **Table 1**. The original DSC curves with key parameter values are all provided in Supplementary data. (**Figure S2-S12**) The obtained phase change materials all have very high enthalpy efficiency (>92 %, Table 1), which may be due to the good compatibility between PLA and PCM work substances. Furthermore, we assigned that its internal nanostructure may well act as a nucleating agent to induce crystallization of PCM work substance according to the high enthalpy efficiency.

The enthalpy efficiency of PCMs can be determined by equation 3, [23]

$$Enthalpy\ efficiency\ \% = \frac{\Delta H_m}{\omega \Delta H_{PCM}} \times 100\ \% \quad (3)$$

where, ΔH_m (J g^{-1}) was the latent heat value of the PCM composites. ΔH_{PCM} (J g^{-1}) represents the latent heat of PCM work substances, and ω (%) represents the mass ratio of work substance in the PCM composites.

PLA7-Paraffin was selected as a typical sample for the cycle performance test, and the corresponding results are shown in **Figure 3f** and **3g**. All the melting enthalpies, phase change temperature (T_m) and solidification temperature (T_s) keep almost constant, and Cycle 1 and Cycle 55 are almost overlapped completely (**Figure S17**), which indicates PCM performed with good cycle stability. Notably, we can use a convenient method of adding thermally conductive fillers in the step of aerogel fabrication to improve the thermal conductivity of the PCM composites. When we add an appropriate amount of BN or GNP fillers to the aerogel, its thermal conductivity can be significantly improved by 14.5% and 62.4%, respectively. (**Figure 3h**)

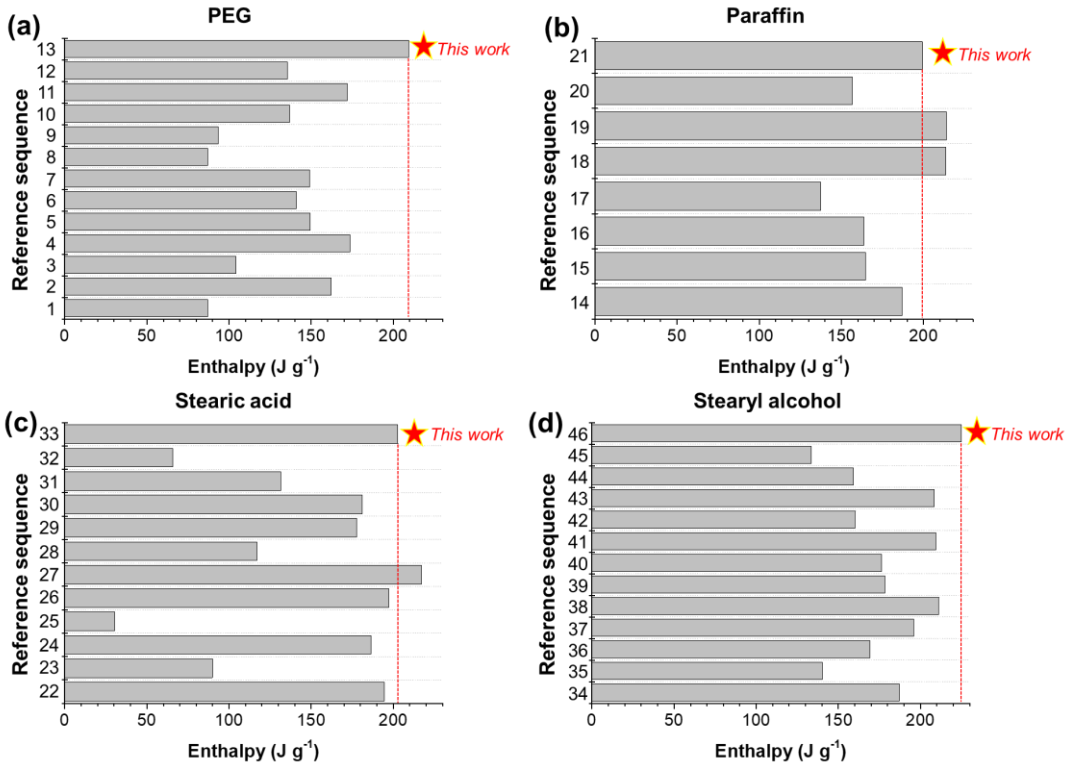

Figure 4. Comparation for latent heat according to the literatures elsewhere: (a) PEG, (b) Paraffin, (c) Stearic acid and (d) Stearyl alcohol. Please note, data shown here are based on optimal metrics reported in the literature listed in Table 2; the reference sequence is following the number in Table 2.

Table 2. Comparison with the preparation method, key parameters for the PEG, Paraffin, Stearic acid and Stearyl alcohol based PCMs in the recent literature elsewhere.

No.	PCM work substance	Supporter materials	Preparation method	PCM loading rate (%)	Enthalpy efficiency (%)	Latent heat (J g^{-1})	References
1	PEG	Poly (Glycerol-Itaconic acid)	Melting copolymerization	72.7	67.9	86.9	[24]
2	PEG	Polyrotaxane	Melting blending	71.4	>100%	116.1–162.2	[25]
3	PEG	Vanadium dioxide	Vacuum	63.9	-	104.3	[26]

			impregnation				
4	PEG	Polyacrylonitrile copolymer	Vacuum melting impregnation	94.4	98.8	173.5	[27]
5	PEG	Graphene oxide and hexagonal boron nitride	Grafted polymerization	-	81.1	149.4	[28]
6	PEG	Toluene diisocyanate	Esterification	89.4	-	141.0	[29]
7	PEG	Melamine foam	Vacuum impregnation	68.5	56.3	148.9	[30]
8	PEG	Poly (glycerol-itaconic acid)	Crosslinking reaction	-	-	86.9	[31]
9	PEG	Lamellar anhydrous calcium sulfate	Vacuum impregnation	-	93.0	93.5	[32]
10	PEG	Poly (butylene terephthalate)	Melting copolymerization	-	83	136.8	[33]
11	PEG	CuS modified PEG	Melt blending	-	-	171.8	[34]
12	PEG	Renewable potatoes	Vacuum impregnation	82.1	91.5	135.6	[35]
13	PEG	PLA aerogel	3D foam encapsulation	94.0	100.1	209.3	Current work
14	Paraffin	Nano-Fe_3O_4	Two-step technique	-	-	187.0	[36]
15	Paraffin	Expanded Graphite	Direct impregnation	-	-	164.8	[37]
16	Paraffin	Diatomite-vermiculite mineral system.	Direct impregnation	-	-	163.7	[38]
17	Paraffin	Copper foam	-	-	-	137.4	[39]
18	Paraffin	Hierarchical porous skeleton material	Vacuum impregnation	78.8	-	213.6	[40]
19	Paraffin	Steel wires	Blend	90	-	213.8	[41]
20	Paraffin	SiO_2	Infiltration	78.2		156.6	[42]
21	Paraffin	PLA aerogel	3D foam encapsulation	92.8	101.2	199.3	Current work
22	Stearic acid	Activated alumina oxide	Physical blending	80.0	-	194.7	[43]
23	Stearic acid	Epoxy aerogel	Vacuum adsorption	-	-	89.9	[44]
24	Stearic acid	Expanded graphite	Melt impregnation	92.0	-	186.4	[45]
25	Stearic acid	Palmitic acid	Melting mixing	80.0	-	30.5	[46]
26	Stearic acid	Expanded graphite	Vacuum adsorption	91.0	-	197.2	[47]

27	Stearic acid	Silicone oil	Emulsification reaction	-	-	217.2	[48]
28	Stearic acid	Sugar beet pulp	Vacuum impregnation	70.0	-	117.0	[49]
29	Stearic acid	Palmitic acid	Melt blending	-	-	177.7	[50]
30	Stearic acid	Two-dimensional montmorillonite	Solution mixing	82.1	-	181.0	[51]
31	Stearic acid	Titanium dioxide	Sol gel method	55.7		131.5	[52]
32	Stearic acid	Silica fume	Vacuum impregnation	-	-	65.6	[53]
33	Stearic acid	PLA aerogel	3D foam encapsulation	93.9	92.3	202.8	Current work
34	Stearyl alcohol	Expanded graphite with Co_3O_4	Melt-blending	-	-	187.0	[54]
35	Stearyl alcohol	Expanded perlite	Vacuum impregnation	-	-	140.2	[55]
36	Stearyl alcohol	Hierarchical porous polymer (HPP)	Vacuum impregnation	75	-	169.1	[56]
37	Stearyl alcohol	Al_2O_3@EG	Melt blending and vacuum adsorption	-	-	195.9	[57]
38	Stearyl alcohol	Nano-silicon carbide, expanded graphite	Melt blending and vacuum adsorption	-	-	211.2	[58]
39	Stearyl alcohol	EG-CuS@ZnO	stirring impregnation	-	-	178.3	[59]
40	Stearyl alcohol	Expandable graphite	Melt blending	90.0	-	176.4	[60]
41	Stearyl alcohol	Nano-TiO_2	Melt stirring	-	-	209.3	[61]
42	Stearyl alcohol	Porous fumed silica	Evaporative solution impregnation	75.0	-	160.3	[62]
43	Stearyl alcohol	3D melamine-derived carbon foam	Physical mixture and vacuum impregnation	-	-	208.3	[63]
44	Stearyl alcohol	Palm triple pressed acid	Melt blending	-	-	159.0	[64]
45	Stearyl alcohol	Activated single walled carbon nanotubes	Mix and evaporate the solvent	-	-	133.4	[65]

46	Stearyl alcohol	PLA aerogel	3D foam encapsulation	92.2	92.0	224.9	Current work

We detailly summarized the supporter materials, encapsulation methods and core indicators of recently published PCMs series (PEG, Paraffin, Stearic acid and Stearyl alcohol) in **Table 2**. The optimal melting enthalpies are displayed and compared in **Figure 4**. It can be found that PLA aerogel has significant encapsulation effects on the four typical types of organic PCM work substances. Specifically, within the scope of recent literatures, the latent heat values are ultra-high for all the PLA encapsulated PCMs in current work. This fully demonstrates the significant advantages of PLA as a universal support material in the field of phase change energy storage. Notably, the advantages of PLA aerogel encapsulation can be summarized as follows: (1) PCM composites have high shape stability; (2) The whole process of the PCM composites is simple and efficient. Preparation of encapsulated aerogels are fabricated by using the efficient phase separation method with modification; (3) Innovative selection of bio-based biodegradable PLA matrix; and (4) the ultra-high enthalpy and enthalpy efficiency of the corresponding PCM composites.

2.4 Engineering understanding of PLA aerogel as a universal PCM support matrix

In this section, we intend to interpret and analyze the encapsulation advantages of PLA aerogels for PCM compared with other polymeric supports. In view of the sustainable development mainstream, we only focus on green polymers, as well reviewed in the previous work, [66] mainly including PLA, PCL, Cellulose, Chitosan [23], PHA, and some other polyesters such as PGA, and PBAT. [24,31] The Flory-Huggins interaction parameter (χ) is one of the most important physical parameters in polymer physics. It reflects the change of interaction energy when polymer and other medium small molecules (e.g., solvent and PCM work substance (especially in melting state)) or

polymer and polymer are mixed. The smaller the χ, the more friendly the interface and the better compatibility. The better the compatibility, the better the interface wettability between PCM work substances and supporter materials, which is accordingly beneficial to suppress the PCM leakage to a certain extent. The χ can be calculated by Eq. 4:

$$\chi = \frac{V_{m,PCM}}{RT_m}\left(\delta_{PCM} - \delta_{Support\ matrix}\right)^2 \quad (4)$$

where, $V_{m,PCM}$ ($cm^3\ mol^{-1}$) is the molar volume of the PCM work substance, R is gas constant with value of 8.314 J K^{-1} Mol^{-1}, T_m (K) is the melting temperature of the PCM work substance, δ_{PCM} $(MJ/m^3)^{1/2}$ and $\delta_{Support\ matrix}$ are the calculated solubility parameters of PCM work substance and polymer matrix, respectively.

Calculations of solubility parameters (Eq. 5 and 6) are provided in the Supplementary data (**Table S3-16**). We use the widely applied Hoy method to calculate the solubility parameters of compounds. Notably, the solubility parameter calculated by the Hoy method of stearic acid is 18.16 $(MJ/m^3)^{1/2}$, as reported in the literature elsewhere. [67] The experimental value of PEG is reported as 19.7-21.5 $(MJ/m^3)^{1/2}$,[68] and the calculated values of PHB was 20.56 $(MJ/m^3)^{1/2}$,[69] which are all in good agreement with the calculation results in this work, indicating the calculation accuracy of Hoy method and its wide application as an analytical method.

For PCM work substance,

$$\delta_{PCM} = (F_t + 277)/V_{m,PCM} \quad (5)$$

For polymer,

$$\delta_{polymer} = \left(F_t + \frac{277}{0.5/\Delta_T}\right)/V_{m,polymer} \quad (6)$$

where, F_t ($(MJ/m^3)^{1/2}/mol$) is the molar attraction function, $V_{m,PCM}$ is the molar volume of PCM work substance, $V_{m,\ polymer}$ is the repeat unit molar volume of the matrix polymer repeat unit,

and Δ_T is a parameter derived by Hoy to demonstrate the difference between small molecule and polymer for polymer solubility parameters prediction.

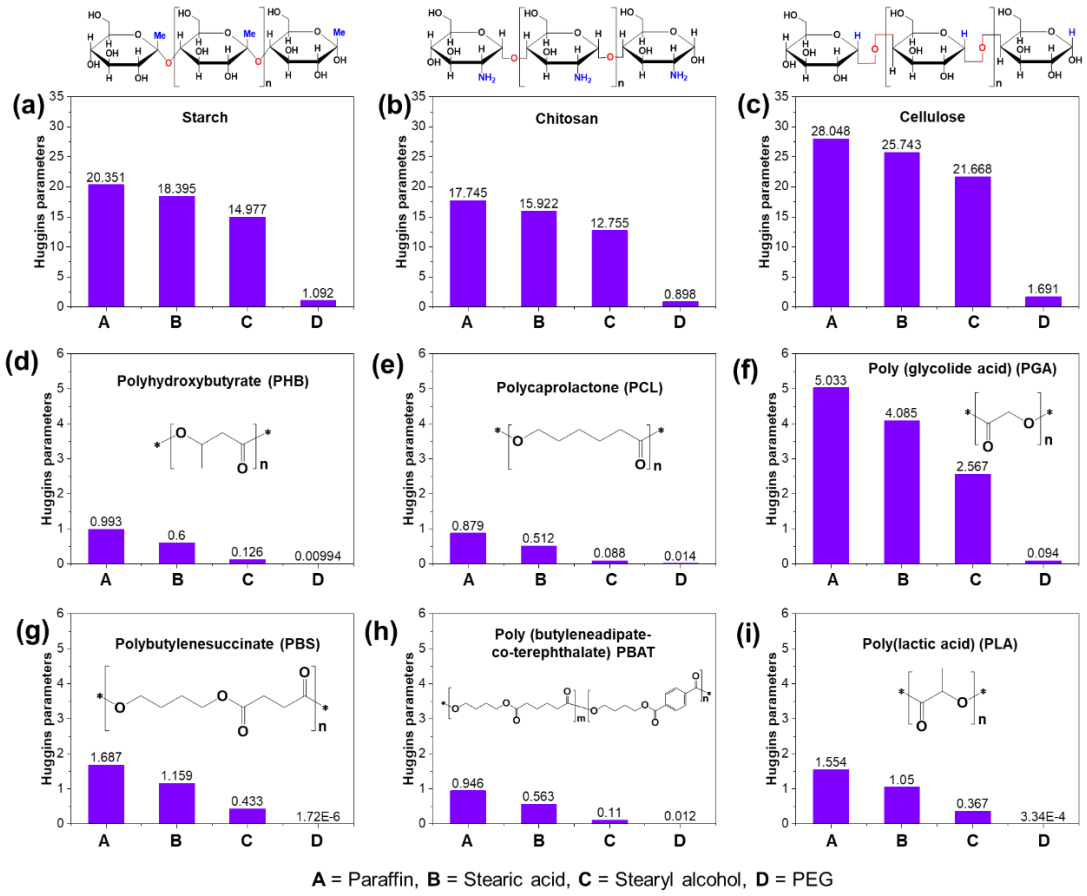

Figure 5. Flory-Huggins parameters of main green polymer matrix to the four typical PCM work substances: (a) Starch, (b) Chitosan, (c) Cellulose, (d) PHB, (e) PCL, (f) PGA, (g) PBS, (h) PBAT, and (i) PLA.

Based on Eq. (4), we can calculate the series of Flory-Huggins parameter, as shown in **Figure 5** and listed in **Table S17**. For a typical example, Cellulose has the highest solubility parameter (32.9 $(MJ/m^3)^{1/2}$), resulting in large Flory-Huggins parameters between common low polar PCM work substances, namely $\chi_{Cellulos-PEG}$, $\chi_{Cellulos-Paraffin}$, $\chi_{Cellulos-Stearic\ Acid}$, and $\chi_{Cellulos-Stearyl\ Acolhol}$ were calculated to be 1.691, 28.048, 25.743 and 21.668, respectively. The low

values of all $\chi_{Cellulos-PEG}$, $\chi_{Chitosan-PEG}$ and $\chi_{Starch-PEG}$ might be the main reason why polysaccharide-based aerogels are mostly used to encapsulate PEG based on the previous reports. [23,70-73] For aliphatic polyesters, it has a solubility parameter like that of most PCM work substances, and with a Flory-Huggins parameter range of 0-5.033 (**Figure 5d-i**), which are much lower than the Flory-Huggins parameters of polysaccharide-based aerogels and typical organic PCM work substances. We believe that poor wettability will affect the adsorption rate as well as the leakage resistance, which may be the main reason why researchers generally choose non-polar substrates for Paraffin encapsulations. We believe that under the same porosity and distribution, the lower Flory-Huggins parameter will be more conducive to the absorption because the interface compatibility. Thus, there is a higher contribution to the resistance to leakage. Please note that here we just analyze the possible advantages of PLA supporter materials, providing a new dimension of understanding on the supporter materials selection. In the actual process, the leakage resistance is also affected by many other factors, such as porosity, void morphology, surface tension, hydrogen bond and internal microstructure.

Based on the calculation results in **Figure 5**, polyester and typical PCM have low Flory-Huggins parameters, according to which, we can predict that the compatibility between all the mentioned polyester and all the four PCM work substances will be excellent. Notably, we believe that PLA is the best one for 3D PCM supporter materials among all the listed sustainable polymers, because the glass transition temperature ($T_{g,\,PLA}$~60 °C) is close to the phase transition temperature of typical organic PCM work substances, which will be conducive to the interfacial compatibility between PLA internal nano units and PCM work substance in melting state; the melting temperature (T_m) is high, which can maintain the 3D structure (form stability) during the PCM melting; it is 100%

environmentally friendly, and the corresponding aerogel preparation is relatively mature and widely used. As shown in **Table S18**, we listed some physical parameters of the corresponding polymers, including solubility, T_g, T_m, and source for the polymers (e.g., PHB, PCL, PGA, PBS and PBAT), to clarify the differences between PLA and the other mentioned polyesters and to proof the advantages of PLA selection accordingly.

2.5 Application cases, limitations, and some strategies of the PLA aerogel encapsulated form sable PCMs

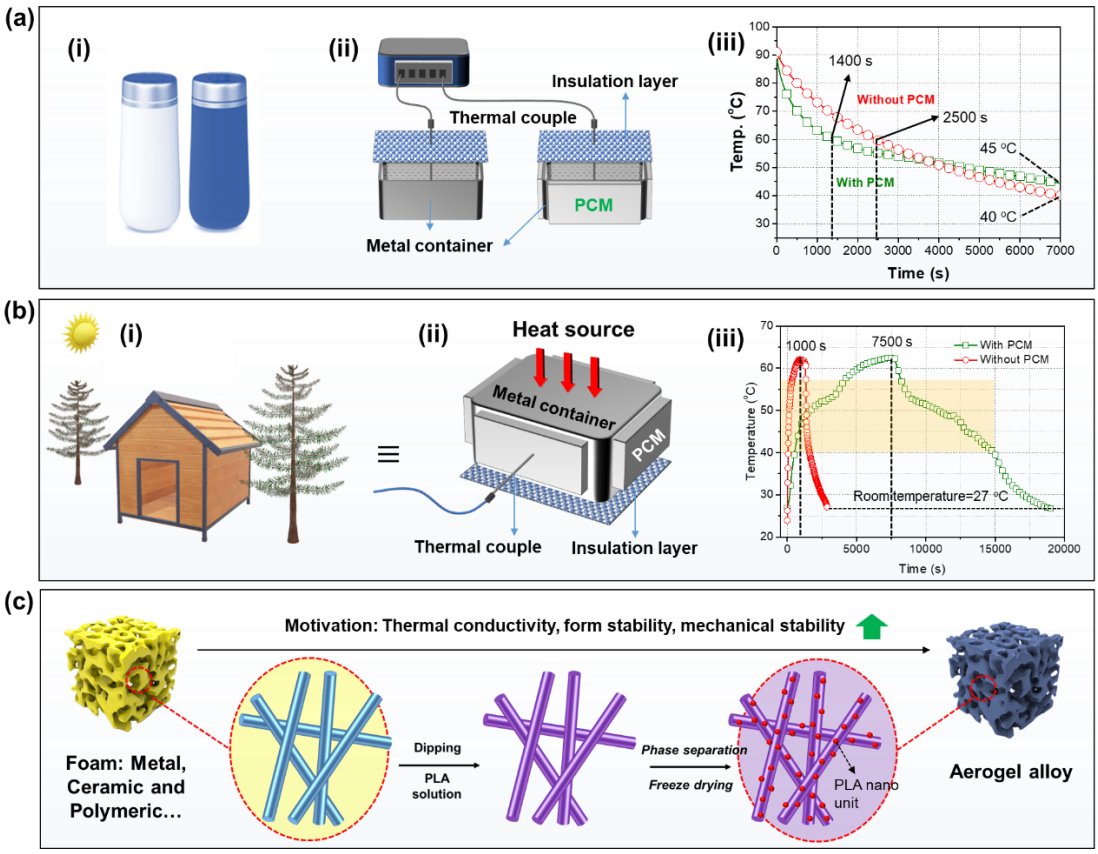

Figure 6. Application exploration: (a)-i, Smart cup, (a)-ii, illustration of smart cup thermal regulation test, (a)-iii, the temperature change curves of the water in the container with and without PCM; (b)-i, illustration of the house as an example for temperature regulation; (b)-ii, the simulated temperature control for a closed space, (b)-iii, the temperature change of the space with and without

PCM; (c) a general strategy to expand the PLA aerogel applications to fabricate: aerogel alloy.

2.5.1 *Application cases*

Considering the possibility of large-scale application and the practical requirements of sustainable development, we choose bio-based stearyl alcohol with the highest melting enthalpy as a typical example to illustrate the practical application possibility and application performance of this phase change material. The test procedures were shown in **Figure S18-19**. As shown in **Figure 6a i-ii**, the control sample is a normal container (without PCM), and the test sample is covered by PCMs (Please see the SI for the details for the test, e.g., the weight of water, the size of PCMs, *etc*.). The temperature change results are shown in **Figure 6a-iii**. As it can be seen, it took 2500 s for the water in the reference container to decrease from 100 ºC to 60 ºC, while the PCM-covered container requires only 1200 s. After 7000s, the temperature can maintain at 45 ºC, and the water temperature of the sample without PCM protection is below 40 ºC. In short, PCM enables the water temperature to make the boiled water drinkable in a shorter period of time, and also keeps the hot water warm for longer period. With the similar principle, application case on temperature regulation in confined spaces are shown in **Figure 6b**. When heated the internal space to the same temperature (62.5 ºC), the required time is 1000 s (without PCM) and 7500 s (with PCM), respectively, indicating that PCM has a good inhibitory effect on the temperature increase in the space. During the cooling process, the samples containing PCM can keep the temperature in the confined space much longer, which demonstrates excellent energy storage and heat retention efficacy. Specifically, the natural cooling times of samples without and containing PCM from 62.5 ºC to room temperature 27 ºC were ~1600 s and ~10000 s, respectively. Its systematic heating or cooling hysteresis can

significantly improve the overall energy efficiency of the building when it is used as a construction material by selecting proper PCM work substance with proper phase transition temperatures.

2.5.2 *Limitations and some strategies*

As a novel supporter material system for high performance PCMs, the composite PCMs reported in current work still suffer some limitations, which are summarized below:

1) Fire safety issues because both the PLA aerogel and the organic PCMs are easily flammable. Thus, it is imperative to improve the fire safety for the current PCMs; [74,75]

2) Mechanical strength and thermal conductivity need to be further enhanced, and

3) Shape stability in large size, e.g., meter scale, which is essential for practical application in construction.

Fortunately, the following strategies can be used for solving the above limitations of corresponding PCMs:

1) Addition of flame retardants (especially the biobased flame retardants) to improve the fire safety.
2) Add high performance thermal conductive fillers, or thermal conductive framework or shaped skeleton, e.g., metal foam or thermal conductive ceramic foams, as illustrated in **Figure 6c**; in addition, other polymeric foam also can be applied for aerogel alloy fabrication, so as to enhance the form stability and mechanical stability.
3) Sandwich layered structure can be designed to further strengthen leakage resistance and mechanical strength.

3. Conclusion

We first prepared a highly porous PLA aerogel based on the method of thermal induced phase

separation-solvent exchange-lyophilization, and its porosity (>90 %) can be achieved by adjusting the concentration of PLA solution. Based on the excellent nanostructure, high porosity and suitable interfacial affinity of PLA aerogel, it is assigned to be excellent support materials for a wide range of typical phase change materials, such as Paraffin, PEG, Stearic acid and Stearyl alcohol), with ultra-high latent heat of 178.9-224.9 J g^{-1}. The obtained phase change material has good hydrophobicity, form stability, leakage resistance, and cycle stability. By using this idea, large scale PLA aerogel can be easily obtained. Therefore, PLA is expected to become an ideal and universal support matrix for high-performance bio-based PCMs. In addition, the thermal conductivity improvement of phase change composites can be achieved by adding thermally conductive fillers (such as BN, GNP, etc.). The solubility parameter of PLA calculated by the Hoy method with calculated value of 21.28 $(MJ/m^3)^{1/2}$, and the low Flory-Huggins parameters, (0.367 for Stearyl Alcohol, 3.34E-4 for PEG, 1.544 for Paraffin, and 1.050 for Stearic acid) are obtained, which we believe is an important factor for the encapsulation universality of PLA. The application cases of smart cups and thermal regulation in space further prove that the high-performance PCMs have remarkable excellent performance and practical application value. In view of such advantages of PLA, we assign that the idea of this aerogel can be compounded for other porous materials (e.g., porous ceramics, metal foams, and other aerogels) to achieve the anti-leakage improvement.

CRediT authorship contribution statement

Guang-Zhong Yin: Conceptualization, Methodology, Validation, Data curation, Writing-original draft, Writing-review & editing, Project administration, Funding acquisition. **Xiao-Mei Yang**: Validation, Data curation, Writing-original draft, Writing-review & editing. **Alba Marta**

López: Data curation, Investigation, Writing-review & editing. **Xiang Ao**: Investigation, Writing-review & editing. **Mei-Ting Wang**: Investigation, Writing-review & editing. **Javier García Molleja**: Data curation, Writing-review & editing. **De-Yi Wang**: Project administration, Methodology, Writing-review & editing, Supervision, Funding acquisition.

Acknowledgment

The authors acknowledge the financial support provided by BIOFIRESAFE Project funded by Ministerio De Ciencia E Innovación (MINECO), Spain with Project number: PID2020-117274RB-I00BIOFIRESAFE, and the internal Fundamental Research Funds of Universidad Francisco de Vitoria (2022).

Declaration of Competing Interest

The authors declare that they have no known competing financial interests or personal relationships that could have appeared to influence the work reported in this paper.

References

1. Huang M, He W, Incecik A, Gupta MK, Królczyk GLi Z, Phase change material heat storage performance in the solar thermal storage structure employing experimental evaluation. Journal of Energy Storage 2022; 46: 103638.
2. Liu W, Bie Y, Xu T, Cichon A, Królczyk GLi Z, Heat transfer enhancement of latent heat thermal energy storage in solar heating system: A state-of-the-art review. Journal of Energy Storage 2022; 46: 103727.
3. Han L, Zhang X, Ji JMa K, Research progress on the influence of nano-additives on phase change materials. Journal of Energy Storage 2022; 55: 105807.
4. Wang S, Wei K, Shi W, Cheng P, Shi JMa B, Study on the rheological properties and phase-change temperature regulation of asphalt modified by high/low-temperature phase change material particles. Journal of Energy Storage 2022; 56: 105970.
5. Abu-Hamdeh NH, Khoshaim A, Alzahrani MAHatamleh RI, Study of the flat plate solar collector's

efficiency for sustainable and renewable energy management in a building by a phase change material: Containing paraffin-wax/Graphene and Paraffin-wax/graphene oxide carbon-based fluids. Journal of Building Engineering 2022; 57: 104804.
6. Nazari N, Bahramian ARAllahbakhsh A, Thermal storage achievement of paraffin wax phase change material systems with regard to novolac aerogel/carbon monofilament/zinc borate form stabilization. Journal of Energy Storage 2022; 50: 104741.
7. Jafaripour M, Sadrameli SM, Pahlavanzadeh HMousavi SAHS, Fabrication and optimization of kaolin/stearic acid composite as a form-stable phase change material for application in the thermal energy storage systems. Journal of Energy Storage 2021; 33: 102155.
8. Li T, Pan H, Xu L, Ni K, Shen YLi K, Shape-stabilized phase change material with high phase change enthalpy made of PEG compounded with lignin-based carbon. International Journal of Biological Macromolecules 2022; 213: 134-44.
9. Liu P, Chen X, Li Y, Cheng P, Tang Z, Lv J, Aftab W, Wang G, Aerogels Meet Phase Change Materials: Fundamentals, Advances, and Beyond. ACS Nano 2022; 16 (10): 15586-626.
10. Cui H, Wang P, Yang HShi Y, Large-scale fabrication of expanded graphite aerogel-based phase change material composite for efficient solar harvesting. Journal of Energy Storage 2022; 56: 105890.
11. Wang K, Zhang T, Wang T, Xu C, Ye FLiao Z, Microencapsulation of high temperature metallic phase change materials with SiCN shell. Chemical Engineering Journal 2022; 436: 135054.
12. Qian T, Li J, Ma HYang J, The preparation of a green shape-stabilized composite phase change material of polyethylene glycol/SiO2 with enhanced thermal performance based on oil shale ash via temperature-assisted sol–gel method. Solar Energy Materials and Solar Cells 2015; 132: 29-39.
13. Gao N, Tang T, Xiang H, Zhang W, Li Y, Yang C, Xia T, Liu X, Preparation and structure-properties of crosslinking organic montmorillonite/polyurethane as solid-solid phase change materials for thermal energy storage. Solar Energy Materials and Solar Cells 2022; 244: 111831.
14. Liao H, Chen W, Liu YWang Q, A phase change material encapsulated in a mechanically strong graphene aerogel with high thermal conductivity and excellent shape stability. Composites Science and Technology 2020; 189: 108010.
15. Pan C, He P, Wu J, Chen N, Wei J, Xu T, Shi E, Wang A, Jia H, Copper foam effectively improves the thermal performance of graphene-aerogel composite phase-change materials for thermal storage. Journal of Energy Storage 2022; 51: 104485.
16. Abbasi Moud A, Advanced cellulose nanocrystals (CNC) and cellulose nanofibrils (CNF) aerogels: Bottom-up assembly perspective for production of adsorbents. International Journal of Biological Macromolecules 2022; 222: 1-29.
17. Cheng G, Wang Z, Wang XHe Y, All-climate thermal management structure for batteries based on expanded graphite/polymer composite phase change material with a high thermal and electrical conductivity. Applied Energy 2022; 322: 119509.
18. Wei P, Cipriani CEPentzer EB, Thermal energy regulation with 3D printed polymer-phase change material composites. Matter 2021; 4 (6): 1975-89.
19. La Carrubba V, Pavia FC, Brucato VPiccarolo S, PLLA/PLA scaffolds prepared via Thermally Induced Phase Separation (TIPS): tuning of properties and biodegradability. International Journal of Material Forming 2008; 1 (1): 619-22.
20. Liu W, Huang N, Yang J, Peng L, Li JChen W, Characterization and application of porous polylactic acid films prepared by nonsolvent-induced phase separation method. Food Chemistry 2022; 373: 131525.
21. Yin G, Zhao D, Zhang L, Ren Y, Ji S, Tang H, Zhou Z, Li Q, Highly porous 3D PLLA materials

composed of nanosheets, fibrous nanosheets, or nanofibrous networks: Preparation and the potential application in oil–water separation. Chemical Engineering Journal 2016; 302: 1-11.
22. Yin G, Zhao D, Ren Y, Zhang L, Zhou ZLi Q, A convenient process to fabricate gelatin modified porous PLLA materials with high hydrophilicity and strength. Biomaterials Science 2016; 4 (2): 310-8.
23. Cheng P, Gao H, Chen X, Chen Y, Han M, Xing L, Liu P, Wang G, Flexible monolithic phase change material based on carbon nanotubes/chitosan/poly(vinyl alcohol). Chemical Engineering Journal 2020; 397: 125330.
24. Yin G-Z, Díaz Palencia JLWang D-Y, Fully bio-based Poly (Glycerol-Itaconic acid) as supporter for PEG based form stable phase change materials. Composites Communications 2021; 27: 100893.
25. Yin G-Z, Marta López A, Yang X-M, Ao X, Hobson JWang D-Y, Polyrotaxane based leakage-proof and injectable phase change materials with high melting enthalpy and adjustable transition temperature. Chemical Engineering Journal 2022; 444: 136421.
26. Bai K, Li C, Xie B, Zhang D, Lv Y, Xiao J, He M, Zeng X, Zeng J, Chen J, Emerging PEG/VO2 dual phase change materials for thermal energy storage. Solar Energy Materials and Solar Cells 2022; 239: 111686.
27. Yin C, Weng L, Fei Z-X, Shi L-YYang K-K, Form-Stable phase change composites based on porous carbon derived from polyacrylonitrile hydrogel. Chemical Engineering Journal 2022; 431: 134206.
28. Jing R, Zhang H, Huang C, Su F, Wu B, Sun Z, Xu F, Sun L, Xia Y, Peng H, Lin X, Li B, Zou Y, Chu H, Huang P, Yan E, Construction of double cross-linking PEG/h-BN@GO polymeric energy-storage composites with high structural stability and excellent thermal performances. Colloids and Surfaces A: Physicochemical and Engineering Aspects 2022; 638: 128193.
29. Zhao Y, Liu T, Wei Z, Zhao S, Lei JFu X, Towards high performance semi-interpenetrating phase change materials networks via linear polyethylene glycol-based multimerization effect. Chemical Engineering Journal 2022; 446: 136982.
30. Xiao Y-y, He Y-j, Wang R-q, Lei Y-z, Yang J-h, Qi X-d, Wang Y, Mussel-inspired strategy to construct 3D silver nanoparticle network in flexible phase change composites with excellent thermal energy management and electromagnetic interference shielding capabilities. Composites Part B: Engineering 2022; 239: 109962.
31. Yin G-Z, Yang X-M, Hobson J, López AMWang D-Y, Bio-based poly (glycerol-itaconic acid)/PEG/APP as form stable and flame-retardant phase change materials. Composites Communications 2022; 30: 101057.
32. Lou J, Zhang K, Qin S, Lei Y, Liu Y, He M, Yu J, Two-dimensional lamellar phosphogypsum/polyethylene glycol composite PCM: Fabrication and characterization. Journal of Industrial and Engineering Chemistry 2022; 113: 431-8.
33. Yan D, Zhao S, Ge C, Gao J, Gu CFan Y, PBT/adipic acid modified PEG solid-solid phase change composites. Journal of Energy Storage 2022; 52: 104753.
34. Dong Y, Liu H, Zhang N, Zhou JPan X, Photo-to-thermal conversion and energy storage of polyethylene glycol/copper sulfide composite PCMs. Solar Energy Materials and Solar Cells 2022; 238: 111583.
35. Fang Y, Liu S, Li X, Hu X, Wu H, Lu X, Qu J, Biomass porous potatoes/MXene encapsulated PEG-based PCMs with improved photo-to-thermal conversion capability. Solar Energy Materials and Solar Cells 2022; 237: 111559.
36. Lu B, Zhang Y, Zhang J, Zhu J, Zhao HWang Z, Preparation, optimization and thermal characterization of paraffin/nano-Fe3O4 composite phase change material for solar thermal energy

storage. Journal of Energy Storage 2022; 46: 103928.
37. Luo Z, Huang Z, Xie N, Gao X, Xu T, Fang Y, Zhang Z, Numerical and experimental study on temperature control of solar panels with form-stable paraffin/expanded graphite composite PCM. Energy Conversion and Management 2017; 149: 416-23.
38. Costa JAC, Martinelli AE, do Nascimento RMMendes AM, Microstructural design and thermal characterization of composite diatomite-vermiculite paraffin-based form-stable PCM for cementitious mortars. Construction and Building Materials 2020; 232: 117167.
39. Hou Y, Chen HLiu X, Experimental study on the effect of partial filling of copper foam on heat storage of paraffin-based PCM. Renewable Energy 2022; 192: 561-71.
40. Wang C, Cheng C, Jin TDong H, Water evaporation inspired biomass-based PCM from daisy stem and paraffin for building temperature regulation. Renewable Energy 2022; 194: 211-9.
41. Wang H, Zhang CYZhang LG, Effect of steel-wires and paraffin composite phase change materials on the heat exchange and exergetic performance of salt gradient solar pond. Energy Reports 2022; 8: 5678-87.
42. Belessiotis GV, Papadokostaki KG, Favvas EP, Efthimiadou EKKarellas S, Preparation and investigation of distinct and shape stable paraffin/SiO2 composite PCM nanospheres. Energy Conversion and Management 2018; 168: 382-94.
43. Chen Y, Xu C, Cong R, Ran FFang G, Thermal properties of stearic acid/active aluminum oxide/graphene nanoplates composite phase change materials for heat storage. Materials Chemistry and Physics 2021; 269: 124747.
44. Bian Y, Wang K, Wang J, Yu Y, Liu MLv Y, Preparation and properties of capric acid: Stearic acid/hydrophobic expanded perlite-aerogel composite phase change materials. Renewable Energy 2021; 179: 1027-35.
45. Ao C, Yan S, Zhao S, Hu W, Zhao LWu Y, Stearic acid/expanded graphite composite phase change material with high thermal conductivity for thermal energy storage. Energy Reports 2022; 8: 4834-43.
46. Dai J, Ma F, Fu Z, Li C, Wu D, Shi K, Dong W, Wen Y, Jia M, Assessing the direct interaction of asphalt binder with stearic acid/palmitic acid binary eutectic phase change material. Construction and Building Materials 2022; 320: 126251.
47. Gao H, Bing N, Xie HYu W, Energy harvesting and storage blocks based on 3D oriented expanded graphite and stearic acid with high thermal conductivity for solar thermal application. Energy 2022; 254: 124198.
48. Delgado-Sánchez C, Partal P, Martín-Alfonso MJNavarro FJ, Oil-in-Oil emulsions of stearic acid dispersed in silicone oil with enhanced energy storage capability for heat transfer fluids. Solar Energy Materials and Solar Cells 2022; 245: 111893.
49. Sarı A, Hekimoğlu G, Karabayır Y, Sharma RK, Arslanoğlu H, Gencel O, Tyagi VV, Capric-stearic acid mixture impregnated carbonized waste sugar beet pulp as leak-resistive composite phase change material with effective thermal conductivity and thermal energy storage performance. Energy 2022; 247: 123501.
50. Zhang NDu Y, Ultrasonic enhancement on heat transfer of palmitic-stearic acid as PCM in unit by experimental study. Sustainable Cities and Society 2018; 43: 532-7.
51. Yi H, Zhan W, Zhao Y, Qu S, Wang W, Chen P, Song S, A novel core-shell structural montmorillonite nanosheets/stearic acid composite PCM for great promotion of thermal energy storage properties. Solar Energy Materials and Solar Cells 2019; 192: 57-64.
52. Li C, He G, Yan H, Yu HSong Y, Synthesis of microencapsulated stearic acid with amorphous TiO2

as shape-stabilized PCMs for thermal energy storage. Energy Procedia 2018; 152: 390-4.
53. Hekimoğlu G, Nas M, Ouikhalfan M, Sarı A, Tyagi VV, Sharma RK, Kurbetci Ş, Saleh TA, Silica fume/capric acid-stearic acid PCM included-cementitious composite for thermal controlling of buildings: Thermal energy storage and mechanical properties. Energy 2021; 219: 119588.
54. Kuai ZH, Yan T, Huo YJ, Wang KPan WG, Thermal characteristics of the multilayered structural MOF-EG/OC composite phase change material in thermal energy storage. Energy and Buildings 2022; 260: 111906.
55. Lv P, Ding M, Liu CRao Z, Experimental investigation on thermal properties and thermal performance enhancement of octadecanol/expanded perlite form stable phase change materials for efficient thermal energy storage. Renewable Energy 2019; 131: 911-22.
56. Tang J, Yang M, Yu F, Chen X, Tan LWang G, 1-Octadecanol@hierarchical porous polymer composite as a novel shape-stability phase change material for latent heat thermal energy storage. Applied Energy 2017; 187: 514-22.
57. Gong S, Cheng X, Li Y, Shi D, Wang XZhong H, Enhancement of ceramic foam modified hierarchical Al2O3@expanded graphite on thermal properties of 1-octadecanol phase change materials. Journal of Energy Storage 2019; 26: 101025.
58. Gong S, Cheng X, Li Y, Wang X, Wang YZhong H, Effect of nano-SiC on thermal properties of expanded graphite/1-octadecanol composite materials for thermal energy storage. Powder Technology 2020; 367: 32-9.
59. Yan T, Li ZHPan WG, 3D network structural shape-stabilized composite PCMs for integrated enhancement of thermal conductivity and photothermal properties. Solar Energy Materials and Solar Cells 2022; 240: 111645.
60. Liu J, Jiang D, Fei H, Xu Y, Zeng ZYe W, Preparation and properties of lauric acid-octadecanol/expanded graphite shape-stabilized phase change energy storage material. Materials Today Communications 2022; 31: 103325.
61. Qin J, Chen Y, Xu CFang G, Synthesis and thermal properties of 1-octadecanol/nano-TiO2/carbon nanofiber composite phase change materials for thermal energy storage. Materials Chemistry and Physics 2021; 272: 125041.
62. Nguyen GT, Do MH, Ly TN, Park IBui TH, Novel shape-stabilized phase change materials: Insights into the thermal energy storage of 1-octadecanol/fumed silica composites. Journal of Energy Storage 2022; 52: 104772.
63. Wang X, Cheng X, Li Y, Li L, Wang Q, Mou F, Yu G, In-situ calcination of NiO nanowalls@carbon foam with hybrid 2D/3D framework to reinforce 1-octadecanol phase change materials. Journal of Energy Storage 2022; 50: 104611.
64. Mhike W, Focke WW, Mackenzie J, Mills EJBadenhorst H, Stearyl alcohol/palm triple pressed acid-graphite nanocomposites as phase change materials. Thermochimica Acta 2018; 663: 77-84.
65. Göksu H, Aydınlı E, Hekimoğlu G, Sarı A, Gencel O, Subaşı S, Tozluoğlu A, Activated carbon nanotube/polyacrylic acid/stearyl alcohol nanocomposites as thermal energy storage effective shape-stabilized phase change materials. Surfaces and Interfaces 2022; 31: 102088.
66. Yin G-ZYang X-M, Biodegradable polymers: a cure for the planet, but a long way to go. Journal of Polymer Research 2020; 27 (2): 38.
67. Bahrami MAFarhadian N, Experimental study and mathematical modeling for encapsulation of fentanyl citrate drug in nanostructured lipid carrier. Journal of Biomolecular Structure and Dynamics 2020; 38 (5): 1263-71.

68. Özdemir CGüner A, Solubility profiles of poly(ethylene glycol)/solvent systems, I: Qualitative comparison of solubility parameter approaches. European Polymer Journal 2007; 43 (7): 3068-93.
69. Terada MMarchessault RH, Determination of solubility parameters for poly(3-hydroxyalkanoates). International Journal of Biological Macromolecules 1999; 25 (1): 207-15.
70. Şentürk SB, Kahraman D, Alkan CGökçe İ, Biodegradable PEG/cellulose, PEG/agarose and PEG/chitosan blends as shape stabilized phase change materials for latent heat energy storage. Carbohydrate Polymers 2011; 84 (1): 141-4.
71. Shen Z, Kwon S, Lee HL, Toivakka MOh K, Preparation and application of composite phase change materials stabilized by cellulose nanofibril-based foams for thermal energy storage. International Journal of Biological Macromolecules 2022; 222: 3001-13.
72. Zhao L, Yang G, Shen C, Mao Z, Wang B, Sui X, Feng X, Dual-functional phase change composite based on copper plated cellulose aerogel. Composites Science and Technology 2022; 227: 109615.
73. Quan B, Wang J, Li Y, Sui M, Xie H, Liu Z, Wu H, Lu X, Tong Y, Cellulose nanofibrous/MXene aerogel encapsulated phase change composites with excellent thermal energy conversion and storage capacity. Energy 2023; 262: 125505.
74. Weng J, Huang Q, Li X, Zhang G, Ouyang D, Chen M, Yuen ACY, Li A, Lee EWM, Yang W, Wang J, Yang X, Safety issue on PCM-based battery thermal management: Material thermal stability and system hazard mitigation. Energy Storage Materials 2022; 53: 580-612.
75. Yin G-Z, Yang X-M, Palencia JLD, Hobson J, López AMWang D-Y, Phytic acid as a biomass flame retardant for polyrotaxane based phase change materials. Journal of Energy Storage 2022; 56: 105853.